Computers and Electronics in Agriculture 103 (2014) 104–113

Contents lists available at ScienceDirect

Computers and Electronics in Agriculture

journal homepage: www.elsevier.com/locate/compag

Multi-temporal mapping of the vegetation fraction in early-season wheat fields using images from UAV

J. Torres-Sánchez *, J.M. Peña, A.I. de Castro, F. López-Granados

Institute for Sustainable Agriculture, IAS-CSIC, P.O. Box 4084, 14080 Córdoba, Spain

ARTICLE INFO

Article history:
Received 7 October 2013
Received in revised form 22 January 2014
Accepted 18 February 2014

Keywords:
Mosaicked image
Digital camera
Classification
Early site-specific weed mapping (ESSWM)
Visible vegetation indices
Narrow row crop

ABSTRACT

Mapping vegetation in crop fields is an important step in remote sensing applications for precision agriculture. Traditional aerial platforms such as planes and satellites are not suitable for these applications due to their low spatial and temporal resolutions. In this article, a UAV equipped with a commercial camera (visible spectrum) was used for ultra-high resolution image acquisition over a wheat field in the early-season period. From these images, six visible spectral indices (CIVE, ExG, ExGR, Woebbecke Index, NGRDI, VEG) and two combinations of these indices were calculated and evaluated for vegetation fraction mapping, to study the influence of flight altitude (30 and 60 m) and days after sowing (DAS) from 35 to 75 DAS on the classification accuracy. The ExG and VEG indices achieved the best accuracy in the vegetation fraction mapping, with values ranging from 87.73% to 91.99% at a 30 m flight altitude and from 83.74% to 87.82% at a 60 m flight altitude. These indices were also spatially and temporally consistent, allowing accurate vegetation mapping over the entire wheat field at any date. This provides evidence that visible spectral indices derived from images acquired using a low-cost camera onboard a UAV flying at low altitudes are a suitable tool to use to discriminate vegetation in wheat fields in the early season. This opens the doors for the utilisation of this technology in precision agriculture applications such as early site specific weed management in which accurate vegetation fraction mapping is essential for crop-weed classification.

1. Introduction

The mapping of the percentage of green vegetation per unit of ground surface, i.e., the vegetation fraction (VF), is a major issue in remote sensing. Monitoring the temporal and spatial variations in the VF in a specific area has many ecological and agricultural applications, such as the identification of land degradation and desertification (Xiao and Moody, 2005), the estimation of the phenological and physiological status of vegetation (Yu et al., 2013) and the prediction of crop yields (Yang et al., 2006), among others. In precision agriculture (PA), quantifying the distribution of VF within a crop-field is a first and crucial step prior to addressing further objectives. One of these objectives is the detection and mapping of weeds in crop fields, with the ultimate goal of applying site-specific weed management (SSWM) techniques and controlling weed patches according to their coverage at each point of the crop-field. In this context, remote imagery for mapping weeds has been traditionally provided by piloted airborne (Castro et al., 2012; Peña-Barragán et al., 2011) or satellite platforms (Castro et al., 2013; Martín et al., 2011). However, these platforms are limited in their ability to provide images with adequate spatial resolution for differentiating crop and weed vegetation in early development stages for early site specific weed management ESSWM) (López-Granados, 2011). In most crop-weed scenarios and for post-emergence herbicide application, the optimal date for weed control is when the crop and weeds are in their seedling growth stages (García Torres and Fernández Quintanilla, 1991), and consequently images at very high spatial resolution (often on the order of mm or very few cm) are needed (Hengl, 2006).

Limitations associated with traditional aerial imagery platforms can be overcome by using Unmanned Aerial Vehicles (UAV), which have been developed in recent years into a new aerial platform for image acquisition with a tremendous potential for mapping vegetation cover for detailed vegetation studies with environmental (Bryson et al., 2010; Laliberte and Rango, 2006) and agricultural objectives (Garcia-Ruiz et al., 2013; Herwitz et al., 2004; Torres-Sánchez et al., 2013). UAVs can fly at low altitudes, allowing them to take ultra-high spatial resolution images (e.g., pixels of a few mm or cm) and to observe small individual plants and patches, which has not previously been possible (Xiang and Tian, 2011). Moreover, UAVs can supply images even on cloudy days, and the

* Corresponding author. Tel.: +34 957499218.
E-mail address: jtorres@ias.csic.es (J. Torres-Sánchez).

http://dx.doi.org/10.1016/j.compag.2014.02.009
0168-1699/

time needed to prepare and initiate the flight is reduced, which allows greater flexibility in scheduling the imagery acquisition. Other advantages of UAVs are their lower cost and their great flexibility of configuration compared with piloted aircraft, which allows the utilisation and testing of low-cost sensors such as conventional digital cameras. For example, there is widespread agreement among researchers that commercial cameras have been a powerful tool for assessing green vegetation cover using on-ground imagery taken with terrestrial platforms (Guijarro et al., 2011; Meyer and Neto, 2008; Romeo et al., 2013) and masts (Motohka et al., 2010; Sakamoto et al., 2011; Yu et al., 2013). Together with their low cost, another advantage of conventional digital cameras is their high resolution, which is needed when working in narrow row crops such as wheat. However, to the best of our knowledge, they have not been used for VF assessment in images collected with an UAV for agricultural proposes.

Image analysis techniques for quantifying vegetation cover are generally based on the use of vegetation indices (VIs) (Xiao and Moody, 2005), which are the product of arithmetic operations performed with spectral information from the radiation reflected by the vegetation at different wavelengths. Information derived from VIs is usually less sensitive to illumination and other factors affecting reflectance (Gitelson et al., 2002). The underlying mechanisms of VIs are well understood, and they emphasise some features of vegetation cover and facilitate obtaining relevant information from digital imagery (Delegido et al., 2013). In images at ultra-high spatial resolution, it is necessary to determine the VI that enhances the differences among pixels containing vegetation and pixels containing non-vegetation, as well as the threshold value that sets the breakpoint between both classes. The classification output is necessary for the thresholding operation, which needs to be optimised for a successful result. There are several automatic methods for threshold calculation, among which Otsu's (Otsu, 1979) method is one of the most utilised for agronomical issues (Guijarro et al., 2011; Meyer and Neto, 2008). It assumes that the image contains two classes of pixels (bare soil and vegetation when considering crop scenarios) and then calculates the optimum threshold based on minimising combined spread (intra-class variance).

To date, VF has been estimated by relating it to VI values in image pixels from airborne and satellite platforms, in which the pixels include vegetated and non-vegetated zones due to the large size (from a few square metres to square kilometres) (Barati et al., 2011; Gitelson et al., 2002). Today, the ultra-high resolution of UAV imagery allows images in which almost every pixel covers only vegetation or bare soil, with a low proportion of pixels representing a mixed coverage. Therefore, VF can be calculated as the percentage of pixels classified as vegetation per unit of ground surface. This is particularly relevant when working with crops such as cereals which are sown in narrow crop rows because the surface distance between such rows is usually not wider than 15–17 cm.

In addition to adequate thresholding and good spatial and temporal resolution, another important issue in VF mapping is accurate spatial and temporal consistency. Spatial stability is needed to assure that VF mapping is accurate in the whole studied area because a VI that works appropriately in only a few zones is useless. Temporal stability is recommendable because it makes it possible to obtain VF maps whenever they are needed. Both parameters make possible the construction of VF maps without any quality loss in the most adequate moment according to the objective.

Although previously reported methods have been mostly applied to on-ground images, they could also be suitable for the remote images captured with UAVs, mainly due to the spatial resolution of on-ground and UAV images being on the same order of magnitude. Investigations about detailed evaluation of remote images captured with UAV platforms and their spectral information or derived vegetation indices with the objective of quantifying VF are currently scarce, although recently Peña et al. (2013) developed a method for weed mapping in early-season maize fields using UAV images.

As part of an overall research program to investigate the opportunities and limitations of UAV imagery in accurately mapping weeds in early season winter wheat, it is crucial to explore the potential of generating VF maps from multiple overlapped frames that were mosaicked as a first step in the proper discrimination of crop rows and weeds. Such an approach should demonstrate the ability to accurately discriminate weeds grown between crop rows to design a field program of ESSWM. Consequently, this work evaluated the accuracy, spatial and temporal consistency and sensitivity of different vegetation indices for a wheat crop that were extracted from visible images acquired with a low-cost camera installed in an UAV flying. We focused on several acquisition dates (temporal analysis) and two different flight altitudes. Additionally, to the best of our knowledge, this is the first work to evaluate the adequate performance of Otsu's thresholding method for VF mapping in UAV imagery.

2. Materials and methods

2.1. Study site

The study was performed in a wheat field with flat ground (average slope <1%) situated at the public farm Alameda del Obispo, in Córdoba (southern Spain, coordinates 37,856N, 4,806W, datum WGS84). The wheat crop was sown on November 22th 2012 at 6 kg ha^{-1} in rows 0.15 m apart, and emergence of the wheat plants started by 15 days after sowing (DAS). The field had an area of about 0.5 ha, and was naturally infested by ryegrass (*Lolium rigidum*), which is a monocotyledoneus weed with an appearance very similar to wheat and an analogous phenological evolution. Weed and crop plants were in the principal stage 1 (leaf development) from the BBCH extended scale (Meier, 2001) in the beginning of the experiment, whereas plants were at the principal stage 2 (tillering) in the last days of the study.

2.2. UAV flights and remote images

A quadrocopter platform with vertical take-off and landing (VTOL), model md4-1000 (microdrones GmbH, Siegen, Germany), was used to collect a set of aerial images at two flight altitudes over the experimental crop-field. This UAV (Fig. 1) is equipped with four brushless motors powered by a battery and can fly by remote control or autonomously with the aid of its Global Position System (GPS) receiver and its waypoint navigation system. The VTOL system makes the UAV independent of a runway, so it can be used in a wide range of different situations. The sensor mounted on the UAV to acquire the imagery was a still point-and-shoot camera, model Olympus PEN E-PM1 (Olympus Corporation, Tokyo, Japan). The camera acquires 12-megapixel images in true colour (Red, R; Green, G; and Blue, B, bands) with 8-bit radiometric resolution and is equipped with a 14–42 mm zoom lens. The camera's sensor is 4032 × 3024 pixels, and the images are stored in a secure digital SD-card. The camera was set to operate in the automatic mode, which adjusts the exposure time (shutter speed) and F-stop (aperture) optimally. Image triggering is activated by the UAV according to the programmed flight route. At the moment of each shoot, the on-board computer system records a timestamp, the GPS location, the flight altitude, and vehicle principal axes (pitch, roll and heading). Detailed information about the configuration of the UAV flights and specification of the vehicle and the camera used can be found in Torres-Sánchez et al. (2013).

Fig. 1. Microdrone MD4-1000 flying over the experimental crop.

The first set of aerial images was collected at 35 DAS, and then sets were collected at 7–10 day intervals; the last set was collected at 75 DAS. Therefore, images were obtained at different growth stages. On every date, two flights were performed at different altitudes: 30 m and 60 m. These flight altitudes resulted in spatial resolutions of 1.14 and 2.28 cm, respectively. The flight routes were programmed into the UAV software so that the vehicle stopped 5 s at every image acquisition point to ensure that the camera took a good light measurement. With this configuration, the flights at 30 m and 60 m altitude took 10 and 5 min, respectively; and the UAV acquired 36 and 10 images at 30 and 60 m flight altitude, respectively.

In the course of the UAV flights, a barium sulphate standard Spectralon® panel (Labsphere Inc., North Sutton, NH, USA) of 1×1 m was also placed in the middle of the field (Fig. 2) to calibrate the spectral data. Digital images captured by each camera channel were spectrally corrected by applying an empirical linear relationship (Hunt et al., 2010). Equation coefficients were derived by fitting digital numbers of the images located in the Spectralon panel to the Spectralon ground values.

2.3. Image mosaicking

A sequence of overlapped images was collected in each flight mission to cover the whole experimental crop-field. An important task prior to image analysis was the combination of all these individual and overlapped images by applying a process of mosaicking. The imagery had a 30% side-lap and a 60% forward-lap to allow correct image mosaicking to generate a complete crop map in the whole study area. Agisoft PhotoScan Professional Edition (Agisoft LLC, St. Petersburg, Russia) was employed in this task. The mosaicking process had three principal steps. The first one was the image alignment, i.e., the software searches for common points in the images and matches them, as well as finding the position of the camera for each image and refining camera calibration parameters. The next step was to build the image geometry. Based on the estimated camera positions and images themselves a 3D polygon mesh, representing the overflown area, was built by PhotoScan software. Once the geometry was constructed, the individual images were projected over it for orthophoto generation. The resultant ortho-mosaicked image must be geometrically interoperable and must shows an accurate crop row matching between both sides of overlapped borderline images, both of which guarantee good performance of the subsequent image analysis.

2.4. Quantification of vegetation fraction

Six VIs and two VI combinations, based on RGB space, were tested for classifying green vegetation pixels in the mosaicked images and quantifying vegetation fraction.

- *Normalized green-red difference index* (Gitelson et al., 2002)

$$\mathrm{NGRDI} = \frac{G - R}{G + R} \tag{1}$$

- *Excess green* (Woebbecke et al., 1995)

$$\mathrm{ExG}(2) = 2g - r - b \tag{2}$$

- *Color index of vegetation* (Kataoka et al., 2003)

$$\mathrm{CIVE} = 0.441r - 0.881g + 0.385b + 18.78745 \tag{3}$$

- *Vegetativen* (Hague et al., 2006)

$$\mathrm{VEG} = \frac{g}{r^a b^{(1-a)}} \text{ with a} = 0.667 \text{ as in its reference} \tag{4}$$

- *Excess green minus excess red* (Camargo Neto, 2004).

$$\mathrm{ExGR} = \mathrm{ExG} - \mathrm{ExR} = \mathrm{ExG} - 1.4r - g \tag{5}$$

- *Woebbecke index* (Woebbecke et al., 1995)

$$\mathrm{WI} = \frac{g - b}{r - g} \tag{6}$$

- *Combination* (Guijarro et al., 2011)

$$\mathrm{COM} = 0.25\mathrm{ExG} + 0.3\mathrm{ExGR} + 0.33\mathrm{CIVE} + 0.12\mathrm{VEG} \tag{7}$$

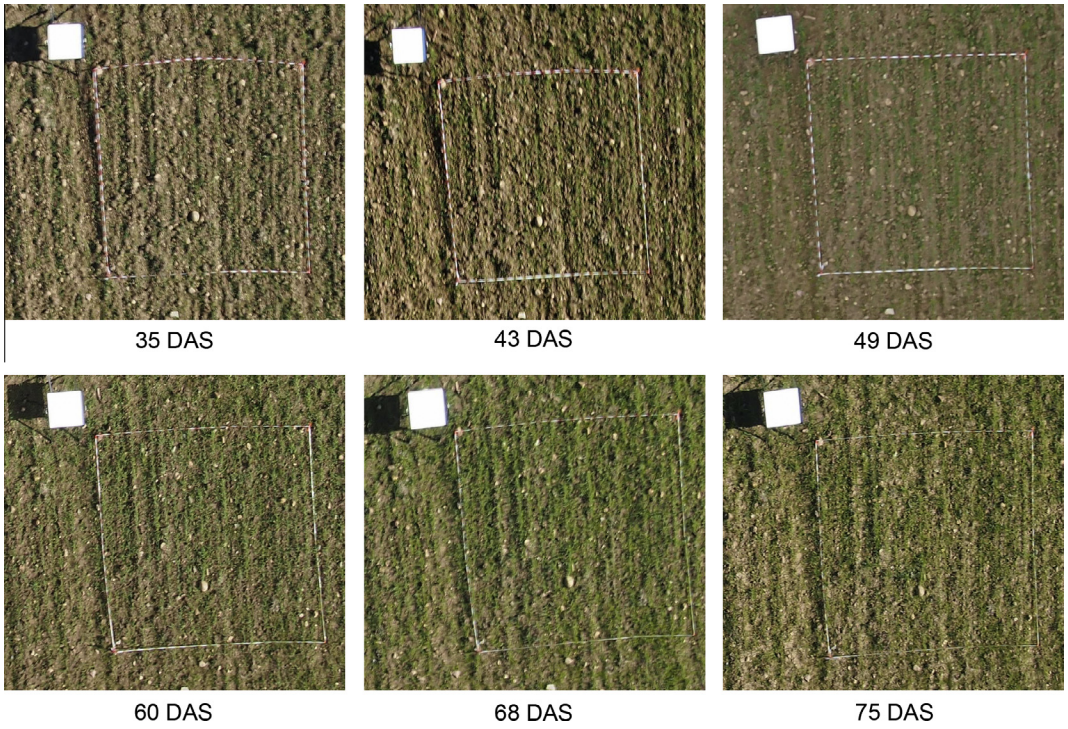

Fig. 2. Spectralon and frames in the wheat field.

- *Combination 2* (Guerrero et al., 2012)

$$\mathrm{COM}(2) = 0.36\mathrm{ExG} + 0.47\mathrm{CIVE} + 0.17\mathrm{VEG} \quad (8)$$

The next normalization scheme was applied in some VIs:

$$r = \frac{R}{R+G+B}; g = \frac{G}{R+G+B}; b = \frac{B}{R+G+B} \quad (9)$$

These VIs were designed to accentuate the green component of the images, and VEG was also designed to cope with the variability of natural daylight illumination. The applications of the VIs were able to transform the images from the original RGB three-band space to a greyscale band. All the mosaicked images from the different dates and flight altitudes were transformed to greyscale images by the application of the above mentioned VIs. In the greyscale images generated by the VIs, pixels corresponding to vegetation zones in the field show intensity levels greater than the rest of the image pixels.

To perform image classification, the value of each greyscale image pixel was compared with a prefixed threshold; if the pixel value was higher than the threshold, then it was classified as vegetation. Once the image pixels were classified, the VF was determined as the percentage of pixels classified as vegetation per unit of ground surface:

$$\mathrm{VF} = \frac{\text{Pixels classified as vegetation(in adelimited area)}}{\text{total pixels(in a delimited area)}} \times 100 \quad (10)$$

The VF was calculated for 96 square frames of three different areas (16, 4 and 1 m^2) distributed regularly throughout the studied surface (Fig. 2). The VF values for every frame were calculated using different thresholds (Table 1) in the greyscale images coming from the application of the studied VIs to all the mosaicked images from every date and flight altitude. The threshold ranges for every index were established to cover the lowest and highest VF values in the whole image. Once the threshold range was established for every VI, it was automatically divided to obtain 10 equidistant values within this range. Then, every one of these 10 values was tested in the determination of VF for 30 and 60 m flight altitude at any flight date.

2.5. Evaluation of VF mapping

For validation purposes, a flight at 10 m altitude was used to collect vertical pictures of the sampling frames. The UAV was programmed to fly continuously taking images every second to obtain several images for every frame, which allowed the choosing of the best one. The high proximity of these images to the frames made it possible to visualise individual plants. Therefore, the best image of every frame was used to extract the observed VF (OVF) data in every sampling point. The accuracy of the VF estimations was evaluated by comparing them with the observed VF values. The observed VF data were determined by using the index and threshold that better detected individual plants according to a visual interpretation (Fig. 3). The following expression was calculated to evaluate the performance of the different indices and thresholds:

$$\mathrm{Accuracy}(\%) = 100 - |\mathrm{OVF} - \mathrm{VF}| \quad (11)$$

The application of Eq. (11) resulted in a high accuracy values. The following statistics from these values were calculated to study the VIs:

- Mean accuracy: calculated for every index as affected by the threshold, flight date, and altitude. It was used to determine the best threshold for every VI for a specific date and flight altitude. Once this threshold was selected, VIs could be compared based on their best operational conditions.
- Standard deviation (SD) of accuracy: calculated for the accuracy values achieved with the best threshold for every index as affected by the flight date and altitude. Every accuracy value was related with a specific frame, so it had coordinates on the field; therefore, the SD measurement of the dispersion from the mean had a spatial meaning in this study. High SD values indicated that the VI accuracy was not stable over the field, with areas in which the VF yielded good estimates and others in which it did not.
- Coefficient of variation (CV): calculated for the best mean accuracies of every VI along the six studied flight dates. It allowed the analysis of how the accuracy of a VI at a flight altitude varied over the time to select the VIs that achieved better classification results without being influenced by the flight date.

Table 1
Thresholds tested to determine the VF for 30 and 60 m flight altitude at any flight date according to the lowest and highest VF values in the mosaicked.

Vegetation indices	Thresholds									
NGRDI	−0.08	−0.06	−0.05	−0.03	−0.01	0.01	0.03	0.05	0.06	0.08
ExG	0.03	0.05	0.08	0.11	0.14	0.16	0.19	0.22	0.25	0.27
CIVE	18.62	18.64	18.65	18.67	18.69	18.71	18.73	18.75	18.76	18.78
VEG	0.90	0.94	0.99	1.03	1.08	1.12	1.17	1.21	1.26	1.30
ExGR	−0.92	−0.90	−0.87	−0.84	−0.81	−0.79	−0.76	−0.73	−0.70	−0.68
COM	6.02	6.04	6.07	6.09	6.11	6.13	6.16	6.18	6.20	6.22
COM2	8.98	9.00	9.02	9.04	9.05	9.07	9.09	9.11	9.12	9.14
WI	−6.11	−4.38	−2.64	−0.90	0.83	2.57	4.30	6.04	7.78	9.51

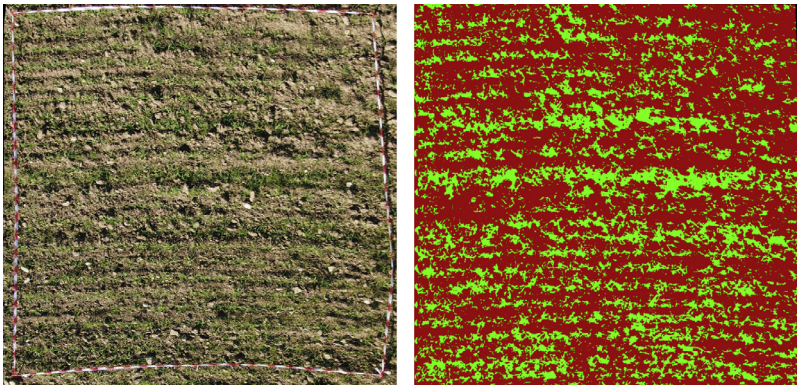

Fig. 3. Ten metre altitude frame image and the output of the image after the vegetation classification process.

After the two best VIs were selected, their accuracy values for the best threshold at every date and flight altitude were distributed in a map using the coordinates of the frames from which they were calculated. Then, using the values at these points, density maps were generated to spatially represent the accuracy of the two VIs at every date and flight altitude. The observed and estimated VFs was also compared for these two VIs using a 1:1 line, which should have a correspondence of 1 in an ideal situation.

The study of the different thresholds and the accuracies achieved with their application to the images allowed the selection of the best VI. Additionally, to evaluate the feasibility of automatic thresholding, Otsu's method (Otsu, 1979) was compared with the best VI from the best date of the experiment. This methodology was developed to be used on grey level histograms, so we tested it on the greyscale band generated by the application of the best VI in the RGB original image. In every validation frame, Otsu's method automatically applied an optimal threshold based on minimizing combined intra-class variance. The results of the VF estimation in both cases, i.e., the best VI threshold and Otsús thresholding, were compared to determine if this methodology was applicable to quantify VF using UAV imagery.

JMP software (SAS, Cary, NC, USA) was employed to perform the data analysis. eCognition Developer 8 (Trimble GeoSpatial, Munich, Germany) was used to automate the VF quantification for all the thresholds, flight altitudes and dates. The Otsu's thresholds were calculated using ImageJ 1.46r (Wayne Rasband, National Institutes of Health, USA).

3. Results

The mean accuracy and the standard deviation at any flight date and altitude was determined using all the VIs with their corresponding 10 thresholds showed in Table 1. The threshold obtaining best results for every VI together to its accuracy and standard deviation at any flight date and altitude are shown in Table 2. At 30 m flight altitude, ExG reached the highest accuracy in the whole experiment on a concrete date (91.99% at 35 DAS); it also had the best mean accuracy for more dates (at 35, 43 and 60 DAS), and it showed the highest mean of accuracy over time (90.20%). At the 60 m flight altitude, Meyer achieved the highest mean accuracy for two dates (43 and 49 DAS), and VEG was also the best for two dates (68 and 75 DAS). The best mean accuracies over the time were reached by VEG (86.25%), closely followed by ExG (86.15%).

3.1. Classification accuracy of VF as affected by VI and spatial factor

Accuracy results were calculated for every georeferenced frame distributed on the field; therefore, the SD values were able to give spatial information about the consistency of VF mean classification accuracy across the experimental field. A low accuracy SD indicated a high spatial consistency of the VI for estimating VF. The lowest SD values were associated in several cases with the highest accuracy at each date and flight altitude, and in the other cases they were associated with the second or third highest accuracy. The ExG, WI and VEG indices showed the lowest SD at one specific date and flight altitude. The index with the best spatial consistency at 30 m and 60 m flight altitude was ExG (7.72 and 10.20, respectively), closely followed by VEG (7.75 and 10.22).

3.2. Classification accuracy of VF as affected by VI and temporal factors

The COM, COM2, ExG, ExGR, NGRDI and VEG indices showed similar accuracy values at all the studied dates; e.g., the ExG mean accuracy only fluctuated between 91.99% and 87.75%. Thus, temporal factors did not have a remarkable influence on the estimation of VF by these indices. However, the CIVE and Meyer accuracies were affected by time, with lower values on the last dates.

The analysis of CV evolution over time was used to determine which VIs showed lower variability over time. This is an important factor to be studied because it is better to use VIs that perform accurate VF quantification regardless of the flight date. The ExG and VEG were the indices with the lowest CVs over the time at the 30 and 60 m flight altitudes, with values of approximately 8.6%, 11.8%, respectively.

Table 2
Mean accuracy (A) and standard deviation (SD) of the accuracy for the best threshold for every index as affected by flight dates and altitudes (m).The mean, standard deviation and coefficient of variation of accuracy for every VI across time are also included.

Index	Flight altitude	Flight dates												Mean A	SD A	CV A (%)
		35 DAS		43 DAS		49 DAS		60 DAS		68 DAS		75 DAS				
		A ± SD	Th	A ± SD	Th	A ± SD	Th	A ± SD	Th	A ± SD	Th	A ± SD	Th			
CIVE	30	83.31 ± 13.27	18.76	80.72 ± 14.58	18.75	79.81 ± 14.89	18.75	76.44 ± 17.02	18.73	75.84 ± 15.64	18.67	66.84 ± 25.21	18.73	77.16	16.77	21.73
	60	80.31 ± 14.51	18.76	75.96 ± 15.88	18.76	76.31 ± 17.14	18.75	72.57 ± 18.12	18.73	69.38 ± 16.28	18.62	62.74 ± 25.90	18.73	72.88	17.97	24.66
COM	30	90.73 ± 7.67	6.09	90.06 ± 8.46	6.11	87.18 ± 10.37	6.09	88.48 ± 8.84	6.13	88.87 ± 7.61	6.11	89.83 ± 7.09	6.13	89.19	8.34	9.35
	60	86.32 ± 9.92	6.09	84.59 ± 10.43	6.11	83.18 ± 13.77	6.09	81.71 ± 14.16	6.13	85.67 ± 10.66	6.13	84.39 ± 10.93	6.11	84.31	11.64	13.81
COM2	30	88.88 ± 7.72	9.04	90.33 ± 8.17	9.04	85.20 ± 11.13	9.02	88.47 ± 7.44	9.07	90.52 ± 7.31	9.05	89.42 ± 8.24	9.05	88.80	8.34	9.39
	60	87.59 ± 10.94	9.02	85.80 ± 10.43	9.04	82.49 ± 13.96	9.02	86.52 ± 10.80	9.05	87.21 ± 9.63	9.05	86.01 ± 9.26	9.05	85.94	10.84	12.61
ExG	30	91.99 ± 6.50	0.11	90.76 ± 7.84	0.14	87.75 ± 9.53	0.11	90.49 ± 6.86	0.19	90.23 ± 7.85	0.16	89.96 ± 7.76	0.16	90.20	7.72	8.56
	60	87.19 ± 11.67	0.08	85.49 ± 12.30	0.11	83.93 ± 10.94	0.11	86.91 ± 9.07	0.16	87.81 ± 8.00	0.14	85.55 ± 9.21	0.16	86.15	10.20	11.84
ExGR	30	91.43 ± 6.63	−0.81	90.03 ± 8.48	−0.79	87.98 ± 9.78	−0.81	87.18 ± 9.76	−0.76	89.17 ± 7.28	−0.79	88.76 ± 8.48	−0.79	89.09	8.40	9.43
	60	84.85 ± 12.72	−0.84	84.28 ± 12.74	−0.81	84.48 ± 12.89	−0.81	83.65 ± 13.08	−0.73	86.62 ± 9.33	−0.76	83.92 ± 10.40	−0.79	84.63	11.86	14.01
WI	30	90.47 ± 6.34	2.64	90.49 ± 8.41	4.36	89.91 ± 8.75	4.36	81.99 ± 15.88	4.36	83.76 ± 10.97	−6.11	77.76 ± 22.07	4.36	85.73	12.07	14.08
	60	87.30 ± 9.81	2.64	88.70 ± 9.14	4.36	88.38 ± 10.16	4.36	76.30 ± 17.51	−2.67	83.76 ± 12.32	−6.11	78.61 ± 20.67	6.07	83.84	13.27	15.83
NGRDI	30	91.45 ± 6.74	−0.03	90.01 ± 8.21	−0.01	88.02 ± 9.81	−0.03	87.66 ± 9.32	0.01	90.03 ± 7.24	−0.01	89.22 ± 7.29	−0.01	89.40	8.10	9.06
	60	85.59 ± 12.12	−0.05	84.69 ± 12.70	−0.03	83.19 ± 13.56	−0.03	82.68 ± 12.26	0.05	82.66 ± 9.31	−0.01	82.84 ± 11.90	−0.03	83.61	11.97	14.32
VEG	30	91.81 ± 6.51	1.12	87.91 ± 8.57	1.21	87.33 ± 9.68	1.12	89.84 ± 7.91	1.21	90.31 ± 6.82	1.17	90.67 ± 6.99	1.21	89.65	7.75	8.64
	60	87.49 ± 10.72	1.08	85.75 ± 12.05	1.12	83.74 ± 10.90	1.12	86.71 ± 9.63	1.21	87.82 ± 8.03	1.17	86.01 ± 10.00	1.17	86.25	10.22	11.85

3.3. Classification accuracy of VF as affected by VI and the flight altitude

The mean accuracies at 30 m of CIVE, COM, COM2, ExG, ExGR, NGRDI and VEG were always higher than at the 60 m flight altitude. Only WI at 75 DAS reached a slightly better accuracy at the 60 m altitude. WI also showed the same accuracy at both flight altitudes at 68 DAS. On average, the accuracy of VF quantification was 3.95% higher at the 30 m altitude. The VI with the greatest accuracy variations associated with flight altitude was NGRDI, whereas the VI that was least affected by this parameter was WI.

3.4. Automatic thresholding by using Otsu's method

Otsu's automatic thresholding methodology was applied to the ExG index for every one of the frames from the 30 m altitude flight at 35 DAS, which was the example in which the best accuracy was achieved. The application of this methodology led to obtaining one threshold by frame, with values ranging from 0.06 to 0.20 and a mean of 0.11. The use of its own threshold for VF quantification in every frame resulted in a mean accuracy of 91.19%, slightly lower than the one calculated using the best threshold from Table 1 (0.11) for ExG in all the frames (91.99%). The mean value of the VI in every frame which is an easy way to obtain a threshold (Burgos-Artizzu et al., 2011; Guijarro et al., 2011), was also tested for thresholding, however it led to an over-estimation of the VF (data not shown). The SD achieved with Otsu's method was 6.95, which indicated a spatial consistency similar to the one obtained using 0.11 as threshold in all the frames (6.50).

3.5. VF mapping from the best VIs

Considering the mean accuracy along all the temporal series, its coefficient of variation, and their spatial consistency, the best VIs were ExG and VEG. Therefore, they were studied more exhaustively. Maps of accuracy by date at the 30 m (Fig. 4) and 60 m flight altitudes (Fig. 5) were built and compared to the maps of the observed VF. The observed VF was also graphically compared with the estimated VF from the 30 and 60 m flights. Prior to the comments on these figures, some details must be clarified as follows:

1. The map size was not the same for all the dates because some images failed to be acquired at 10 m flight altitude, and consequently, there were some small areas in that were unfeasible to use to determine the observed VF.
2. The observed VF was lower on the last date than in the previous one, and this lower vegetation density was even visually apparent in the images. According to the field crop data recorded by the authors on the different flight dates, this could be due to the wheat and weed plants being at the beginning of the tillering growth stage, in which the wheat stems become more vertical and show fewer surfaces in the aerial images (C. Fernández-Quintanilla, personal communication, May 16, 2013).

Accuracy maps were almost identical for both VIs at every flight date. The mapping of accuracy revealed that there was a high proportion of the wheat field in which the accuracy was over 90%, indicating the suitability of the studied VIs for VF quantification. This proportion was lower in imagery acquired at the 60 m flight altitude, as suggested by the lower accuracy values shown in Table 2. Zones with lower accuracy were located at the same places at both 30 and 60 m, but they were bigger at

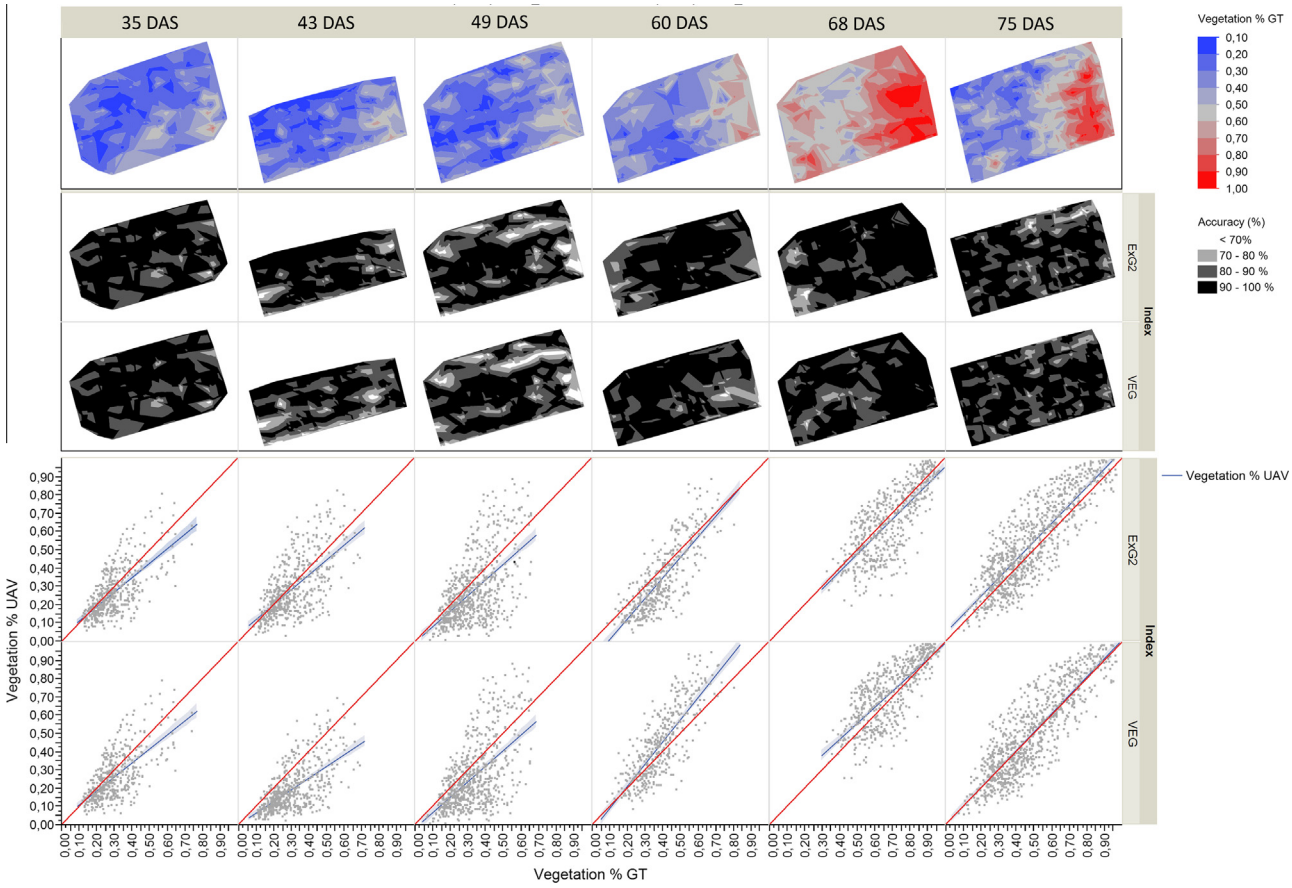

Fig. 4. Observed VF map. Accuracy maps for the best VIs, and graphics comparing the observed and estimated VFs at the 30 m flight altitude.

the higher altitude. Zones with lower accuracy were not consistent over time.

The graphical comparison of the observed and estimated VFs showed that most points were near the 1:1 line, which indicated a high correlation among them. On the first dates, the point cloud and the regression line did not cover the whole range of possible values because there were no frames with high VF values. At 68 DAS, as it was mentioned above, VF reached the highest values; therefore, there were no points in the graphic zone corresponding to lower VF values. The best fit between the regression line and the 1:1 line was reached at the three last dates at the 30 m flight altitude for ExG and VEG. At the 60 m flight altitude, the best fit was also reached at the three last dates for the two studied VIS.

4. Discussion

The discrimination of vegetation in narrow crop row fields during the early growth stages, when the crop row width is 15 cm and the plant size is only of a few centimetres, requires the use of images with a ultra-high spatial resolution because at least four pixels are required to detect the smallest objects within an image (Hengl, 2006). For this reason, distinguishing small seedlings has been commonly undertaken by analyzing images captured with cameras or sensors mounted in on-ground platforms (Burgos-Artizzu et al., 2010; Romeo et al., 2013). However, the use of remote images captured with UAVs flying at low altitudes offer a new opportunity that needs to be investigated in detail. This article shows the visible vegetation indices that best performed green vegetation discrimination in a wheat field tested on six different dates throughout the earliest stages of crop development and compared the results obtained in remote images captured at two different flight altitudes.

Although most VIs tested showed the ability to discriminate vegetation, two indices (ExG and VEG) had the highest classification accuracy independent of the image acquisition date. When mapping spatially variable features in precision agriculture, such as VF or vegetation vigour, good accuracy is needed. However, it is also required that this accuracy be homogenously distributed across the studied crop. Mapping these variables would be useless if the mapping accuracy differed from one zone to another. Therefore, the spatial consistency achieved for ExG and VEG makes them adequate for precision agriculture applications in which vegetation quantification is needed. Yu et al. (2013) also reported that ExG was the VI with the best accuracy in their experiments in maize, closely followed by ExGR and VEG. The excellent fitting between the regression line and the 1:1 line in Figs. 4 and 5 for the three last dates indicates that there is a low probability of under or over-estimation of the vegetation fraction. The worse fitting achieved on the first dates could be due to the lack of points in the graphic region corresponding to high VF values, which causes the accumulation of points in the opposite region of the graphic, while on the three last dates, there were points distributed all over the graphic.

From an agronomic point of view, temporal consistency evaluated by the CV of the accuracy is also of great importance because it allows overflying the crop just when the farmer wants to study the crop without loss in the accuracy of the VF quantification. For example, if the farmer's objective is to detect vegetation as a step prior to designing an early site-specific weed treatment, the crop images can be acquired a few days before the weed treatment is going to be applied.

Meyer and Neto (2008) reported that ExGR does not require a special threshold calculation in images acquired at 1 m above the

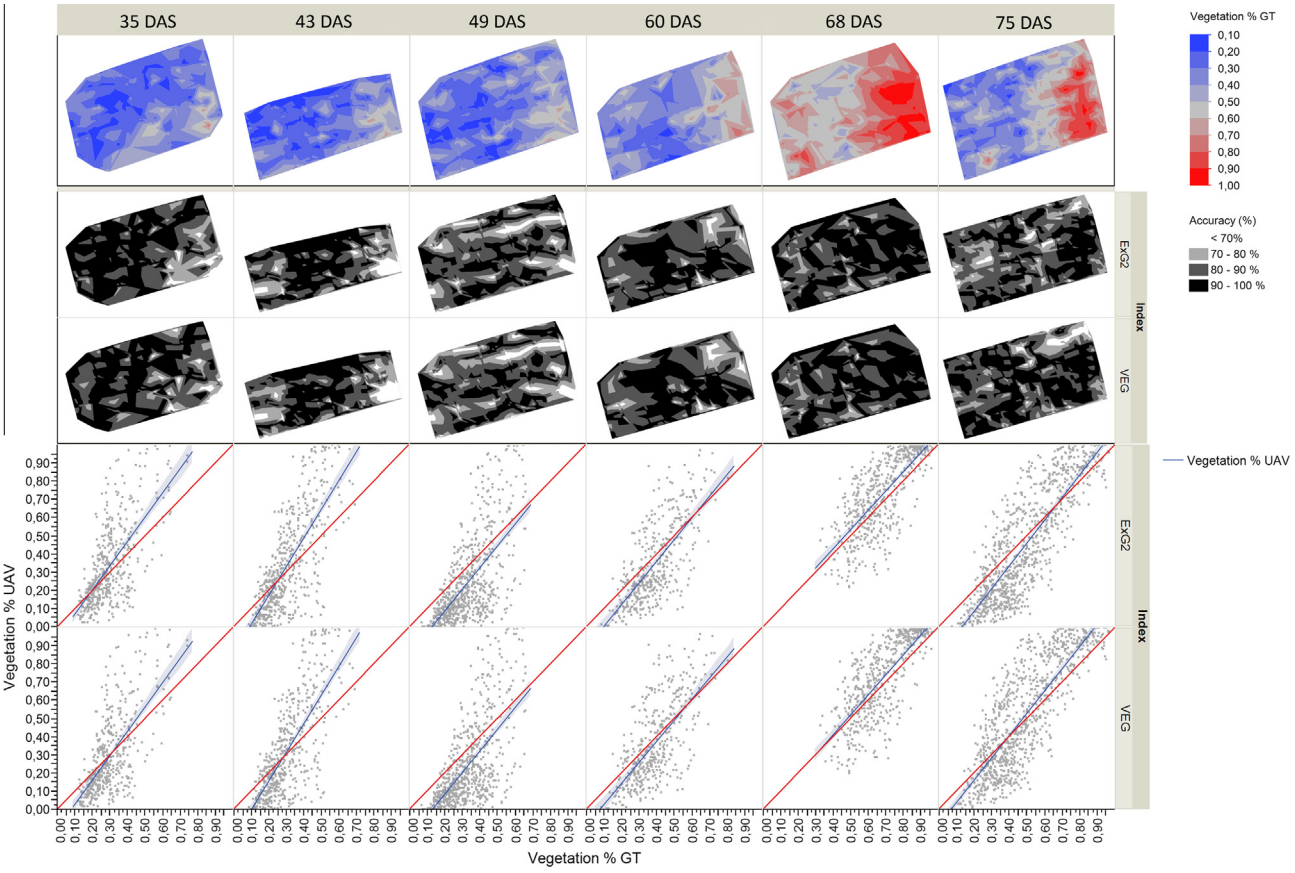

Fig. 5. Observed VF map. Accuracy maps for the best VIs, and graphics comparing the observed and estimated VFs at the 60 m flight altitude.

ground. Their results showed that plant pixel values were all positive, and the remaining background pixels were all negative. However, for the UAV imagery studied in this work, different threshold values lower than zero (i.e., negative) were needed to classify vegetation pixels using ExGR. Those that involved a single threshold were not applicable in our work for every VI, but rather the different dates and flight altitudes analysed made it necessary to search for the best threshold in every case. Guijarro et al. (2011) and Burgos-Artizzu et al. (2011) working with on-ground imagery in maize crops stated that Otsu's thresholding method led to an under-estimation of vegetation in their image analysis. However, Otsu's thresholding method achieved a satisfactory accuracy for the results in our work with remote imagery. Considering the fact that different thresholds were needed for each VI and flight date, Otsu's method could be used to automate the threshold selection in future works where vegetation segmentation from UAV images is required.

Of relevant interest is the definition of the optimum pixel size needed according to the size of the plants to be discriminated. In remote sensing, the pixel size is directly proportional to the flight altitude. In our experiment, classification results were moderately affected by the flight altitude, with an average reduction of 3.95% in the classification results when flight altitudes increased from 30 m (1.14 cm/pixel) to 60 m (2.28 cm/pixel). When the spatial resolution is very high, the plants in the image are well delimited; however, when the spatial resolution is poorer, limits between plants and soil are fuzzy, and consequently, there is usually a higher proportion of pixels including information for both vegetation and bare soil. In our study, this mixed spectral information altered the VI values in those pixels affecting the accuracy of the VF detection. Excluding the pixels with mixed spectral information, the discrimination of pixels corresponding to bare soil or vegetation can be robustly performed because they have two different dominant spectral signatures, green for plants and red for soil (Guerrero et al., 2012). This spectral difference appears even in cases in which the leaf angle and small scale soil properties disrupt the homogeneity of these classes.

In a practical application of these VIs to VF quantification the selection of the flight altitude will depend on several factors, not only on the accuracy of the quantification. Therefore, the loss of about a 4% of accuracy could be assumed by the user if other important advantages are achieved by flying at 60 m instead of flying at 30 m altitude, as described before by Torres-Sánchez et al. (2013). For example, flying at 60 m allows the duplication of the area that can be overflown without problems related with the UAV's energy autonomy. This would reduce the number of images needed to cover the whole studied crop, making it possible to map the VF in a shorter time. If the purpose for VF mapping is ESSWM, the accuracy loss could be overcome by creating a buffer around the detected weeds, which will reduce the chance of missing isolated weeds.

The study of VF in wheat fields in the early season could be used for the detection and mapping of weeds for ESSWM. Crops do not cover the soil entirely in the first growth stages, so if there are regions with low and high VF at early season in a crop field, it can be assumed that the regions with a high percentage of vegetation are infested by weeds. In this stage, mapping weeds in wheat using remote sensing presents much greater difficulties than in the case of the late-stage season for three main reasons (López-Granados, 2011): (1) weeds are generally distributed in small patches, which makes it necessary to work with remote images at very small pixel sizes, often on the order of centimetres (Robert, 1996); (2) grass

weeds and monocotyledonous crops (e.g., *Avena* spp. or *Lolium* spp. in wheat) or broad-leaved weeds and many dicotyledonous crops (e.g., *Chenopodium* spp. in sunflower) generally have similar reflectance properties early in the season, which decreases the possibility of discriminating between vegetation classes using only spectral information; and (3) soil background reflectance may interfere with detection (Thorp and Tian, 2004). The usual first step of the image processing is to separate plants (weeds and crop) from soil, and the second step is to discriminate between crop and weed plants (Peña et al., 2013; Torres-Sánchez et al., 2013). However, the difficulty of mapping early weeds in wheat fields (or other cereals sown in narrow crop rows) is related to the very small distance between crop rows (usually no greater than 15 cm) and the quick growth of these crops in the early growth stages, which cover the inter-row area in a few days, thus reducing the likelihood of weed detection.

Research about the evaluation of factors affecting the application of UAV platforms in weed science is still scarce. Some efforts are being made by the research community for the monitoring of crop growth or weed infestation in early stages using UAV images, although currently most of these investigations only show potential uses (Rasmussen et al., 2013) or are based on results with limited validation (Samseemoung et al., 2012). The influence of the spatial and spectral resolution of the UAV imagery in a multi-temporal study was evaluated in detail in our work. These factors were studied deeply under field conditions, and the results were evaluated with a complete validation set of 96 sampling frames in each of the six studied dates. Although sampling is a hard task in field conditions, it is absolutely needed for an objective evaluation of the results; otherwise the results can only be based on subjective interpretation. Moreover, investigations should also include all the operations needed to generate a whole georeferenced image of the studied field, including the mission planning and image mosaicking, because the advantage of UAV technology in comparison to other remote platforms is the ability to use mosaicked images to map large fields (Torres-Sánchez et al., 2013).

5. Conclusions

Visible spectral indices derived from imagery acquired from an UAV equipped with a low cost camera flying at low altitudes have shown the ability to discriminate vegetation in wheat fields in the early season. Among the tested indices, the two most successful were ExG and VEG, with ExG being the best for practical and farming applications due to its greater simplicity and its satisfactory mean accuracy and SD accuracy at 30 and 60 m flight altitudes for any image acquisition date. Therefore, the altitude and date to perform the flight depend on other parameters, such as the area to be flown over or the objective of the image acquisition.

Otsu's thresholding method can be applied to automatically determine the VI value that performs an adequate discrimination of vegetation. It achieves good accuracy results and allows the automation of the threshold selection, which is one of the key steps in vegetation discrimination through VIs.

The methodology presented herein could be used for mosaicking a range of small to large areas depending on the autonomy of the UAV. This advantage, together with the high temporal resolution and the ultra-high spatial resolution obtained within a range of 2.47–0.74 cm, would allow a greater extension of the detail in the information extracted from the images for weed patch detection, which is the final objective of the research described herein. An accurate VF quantification at very high spatial resolution, like that obtained in this study, can be useful in precision agriculture for different crop monitoring proposes. In the field of ESSWM, the VF maps could be linked to weed infestation, if it is assumed that a higher VF is related to the presence of weeds.

In conclusion, the most important achievement of this study was obtaining accurate VF georreferenced maps in wheat fields at the seedling stage with very high spatial resolution for further use in ESSWM using the ExG vegetation index obtained using an UAV and a low-cost camera. As stated in this paper, the flight altitude had very little effect on the accuracy of the performance of ExG, which is the most appropriate VI for mapping VF due to its high accuracy and its spatial and temporal consistency. The VF quantification through UAV images opens the door to further investigations, whose main objective should consist of the discrimination of the wheat row structure for further identification of weed and crop plants, because the position of each plant relative to the crop rows might be the key feature used to distinguish between the weeds and crop plants. The reasoning behind this objective would be that once crop rows are mapped, if there is vegetation between them, this vegetation is most likely weed plants or weed patches, and thus, weeds could be discriminated and mapped.

Acknowledgments

This research was partly financed by the TOAS Project (Marie Curie Program, ref.: FP7-PEOPLE-2011-CIG-293991, EU-7th Frame Program) and the RHEA project (NMP-CP-IP 245986-2, EU-7th Frame Program). Research of Dr. de Castro and Mr. Torres-Sánchez was financed by JAEPre and FPI Programs, respectively.

References

Barati, S., Rayegani, B., Saati, M., Sharifi, A., Nasri, M., 2011. Comparison the accuracies of different spectral indices for estimation of vegetation cover fraction in sparse vegetated areas, Egypt. J. Remote Sens. Space Sci. 14, 49–56.
Bryson, M., Reid, A., Ramos, F., Sukkarieh, S., 2010. Airborne vision-based mapping and classification of large farmland environments. J. Field Robot. 27, 632–655.
Burgos-Artizzu, X.P., Ribeiro, A., Guijarro, M., Pajares, G., 2011. Real-time image processing for crop/weed discrimination in maize fields. Comput. Electron. Agric. 75, 337–346.
Burgos-Artizzu, X.P., Ribeiro, A., Tellaeche, A., Pajares, G., Fernández-Quintanilla, C., 2010. Analysis of natural images processing for the extraction of agricultural elements. Image Vis. Comput. 28, 138–149.
Camargo Neto, J., 2004. A combined statistical-soft computing approach for classification and mapping weed species in minimum-tillage systems. ETD Collect. Univ. Neb. – Linc. pp. 1–170.
de Castro, A.I., López-Granados, F., Jurado-Expósito, M., 2013. Broad-scale cruciferous weed patch classification in winter wheat using QuickBird imagery for in-season site-sitespecific control, 2013. Precis. Agric. 14, 392–413.
de Castro, A.I., Jurado-Expósito, M., Peña-Barragán, J.M., López-Granados, F., 2012. Airborne multi-spectral imagery for mapping cruciferous weeds in cereal and legume crops. Precis. Agric. 13, 302–321.
Delegido, J., Verrelst, J., Meza, C.M., Rivera, J.P., Alonso, L., Moreno, J., 2013. A red-edge spectral index for remote sensing estimation of green LAI over agroecosystems. Eur. J. Agron. 46, 42–52.
García Torres, L., Fernández Quintanilla, C., 1991. Fundamentos Sobre Malas Hierbas y Herbicídas. Ministerio de Agricultura, Pesca y Alimentación, Servicio de Extensión Agraria.
Garcia-Ruiz, F., Sankaran, S., Maja, J.M., Lee, W.S., Rasmussen, J., Ehsani, R., 2013. Comparison of two aerial imaging platforms for identification of Huanglongbing-infected citrus trees. Comput. Electron. Agric. 91, 106–115.
Gitelson, A.A., Kaufman, Y.J., Stark, R., Rundquist, D., 2002. Novel algorithms for remote estimation of vegetation fraction. Remote Sens. Environ. 80, 76–87.
Guerrero, J.M., Pajares, G., Montalvo, M., Romeo, J., Guijarro, M., 2012. Support vector machines for crop/weeds identification in maize fields. Exp. Syst. Appl. 39, 11149–11155.
Guijarro, M., Pajares, G., Riomoros, I., Herrera, P.J., Burgos-Artizzu, X.P., Ribeiro, A., 2011. Automatic segmentation of relevant textures in agricultural images. Comput. Electron. Agric. 75, 75–83.
Hague, T., Tillett, N.D., Wheeler, H., 2006. Automated crop and weed monitoring in widely spaced cereals. Precis. Agric. 7, 21–32.
Hengl, T., 2006. Finding the right pixel size. Comput. Geosci. 32, 1283–1298.
Herwitz, S., Johnson, L., Dunagan, S., Higgins, R., Sullivan, D., Zheng, J., Lobitz, B., Leung, J., Gallmeyer, B., Aoyagi, M., Slye, R., Brass, J., 2004. Imaging from an unmanned aerial vehicle: agricultural surveillance and decision support. Comput. Electron. Agric. 44, 49–61.

Hunt Jr., E.R., Hively, W.D., Fujikawa, S.J., Linden, D.S., Daughtry, C.S.T., McCarty, G.W., 2010. Acquisition of NIR-green–blue digital photographs from unmanned aircraft for crop monitoring. Remote Sens. 2, 290–305.

Kataoka, T., Kaneko, T., Okamoto, H., Hata, S., 2003. Crop growth estimation system using machine vision. In: 2003 IEEE/ASME International Conference on Advanced Intelligent Mechatronics, 2003. AIM 2003. Proceedings. Presented at the 2003 IEEE/ASME International Conference on Advanced Intelligent Mechatronics, 2003. AIM 2003. Proceedings, pp. b1079–b1083, vol. 2.

Laliberte, A., Rango, A., 2006. Unmanned Aerial Vehicles (UAVs) for Rangeland Remote Sensing. In: Presented at the 3rd Annual Symposium research Insights in Semiarid Ecosystems RISE.

López-Granados, F., 2011. Weed detection for site-specific weed management: mapping and real-time approaches. Weed Res. 51, 1–11.

Martín, M.P., Barreto, L., Fernández-Quintanilla, C., 2011. Discrimination of sterile oat (Avena sterilis) in winter barley (Hordeum vulgare) using QuickBird satellite images. Crop Prot. 30, 1363–1369.

Meier, U., 2001. BBCH Monograph: Growth stages for mono- and dicotyledonous plants. Blackwell Wiss.-Verlag, Berlin.

Meyer, G.E., Neto, J.C., 2008. Verification of color vegetation indices for automated crop imaging applications. Comput. Electron. Agric. 63, 282–293.

Motohka, T., Nasahara, K.N., Oguma, H., Tsuchida, S., 2010. Applicability of green–red vegetation index for remote sensing of vegetation phenology. Remote Sens. 2, 2369–2387.

Otsu, N., 1979. A threshold selection method from gray-level histograms. IEEE Trans. Syst. Man Cybern. 9, 62–66.

Peña, J.M., Torres-Sánchez, J., de Castro, A.I., Kelly, M., López-Granados, F., 2013. Weed Mapping in Early-Season Maize Fields Using Object-Based Analysis of Unmanned Aerial Vehicle (UAV) Images. PLoS ONE 8, e77151.

Peña-Barragán, J.M., Ngugi, M.K., Plant, R.E., Six, J., 2011. Object-based crop identification using multiple vegetation indices, textural features and crop phenology. Remote Sens. Environ. 115, 1301–1316.

Rasmussen, J., Nielsen, J., Garcia-Ruiz, F., Christensen, S., Streibig, J.C., 2013. Potential uses of small unmanned aircraft systems (UAS) in weed research. Weed Res. 53, 242–248.

Robert, P.C., 1996. Use of remote sensing imagery for precision farming. In: Proceedings of 26th International Symposium on Remote Sensing of Environment and 18th symposium of the Canadian Remote Sensing Society, Ontario, Canada, pp. 596–599.

Romeo, J., Pajares, G., Montalvo, M., Guerrero, J.M., Guijarro, M., de la Cruz, J.M., 2013. A new expert system for greenness identification in agricultural images. Exp. Syst. Appl. 40, 2275–2286.

Sakamoto, T., Shibayama, M., Kimura, A., Takada, E., 2011. Assessment of digital camera-derived vegetation indices in quantitative monitoring of seasonal rice growth. ISPRS J. Photogramm. Remote Sens. 66, 872–882.

Samseemoung, G., Soni, P., Jayasuriya, H.P.W., Salokhe, V.M., 2012. Application of low altitude remote sensing (LARS) platform for monitoring crop growth and weed infestation in a soybean plantation. Precis. Agric. 13, 611–627.

Thorp, K.R., Tian, L.F., 2004. A review on remote sensing of weeds in agriculture. Precis. Agric. 5, 477–508.

Torres-Sánchez, J., López-Granados, F., De Castro, A.I., Peña-Barragán, J.M., 2013. Configuration and specifications of an unmanned aerial vehicle (UAV) for early site specific weed management. PLoS One 8, e58210.

Woebbecke, D.M., Meyer, G.E., Von Bargen, K., Mortensen, D.A., 1995. Color indices for weed identification under various soil, residue, and lighting conditions. Trans. ASAE 38, 259–269.

Xiang, H., Tian, L., 2011. Development of a low-cost agricultural remote sensing system based on an autonomous unmanned aerial vehicle (UAV). Biosyst. Eng. 108, 174–190.

Xiao, J., Moody, A., 2005. A comparison of methods for estimating fractional green vegetation cover within a desert-to-upland transition zone in central New Mexico, USA. Remote Sens. Environ. 98, 237–250.

Yang, C., Everitt, J.H., Bradford, J.M., 2006. Comparison of QuickBird satellite imagery and airborne imagery for mapping grain sorghum yield patterns. Precis. Agric. 7, 33–44.

Yu, Z., Cao, Z., Wu, X., Bai, X., Qin, Y., Zhuo, W., Xiao, Y., Zhang, X., Xue, H., 2013. Automatic image-based detection technology for two critical growth stages of maize: emergence and three-leaf stage. Agric. For. Meteorol. 174–175, 65–84.